GEOPHYSICAL RESEARCH LETTERS, VOL. 26, NO. 10, PAGES 1369-1372, MAY 15, 1999

Tidal influences on O_2 atmospheric band dayglow: HRDI observations vs. model simulations

Daniel R. Marsh, Wilbert R. Skinner

Dept. Atmospheric, Oceanic and Space Sciences, University of Michigan, MI

Valery A. Yudin

Institute for Terrestrial and Planetary Atmospheres, State University of New York at Stony Brook, NY

Abstract. Atmospheric tides perturb the temperature, winds, density, and composition of the mesosphere and lower thermosphere (MLT) and therefore affect daytime O_2 atmospheric band airglow. O_2 atmospheric band dayglow measurements made by the High Resolution Doppler Imager (HRDI) show clear tidal signatures in equatorial emission rates during equinox, when diurnal tide amplitudes are large. During solstice the observed symmetric diurnal variation of dayglow indicates an emission process controlled by solar absorption. Observations are compared with modeled emissions based on an atmosphere perturbed with diurnal tides predicted by the Tuned Mechanistic Tidal Model (TMTM) for March 1993. Good data/model agreement indicates enhanced emissions result from tidal advection of atomic oxygen from the lower thermosphere. While tides modulate O_2 nightglow by perturbing atomic oxygen recombination rates, the tidal signatures seen in O_2 dayglow are due to increased production of ozone and $O(^1D)$. These results provide further confirmation of the consistency of the HRDI daytime wind, temperature and airglow observations.

Introduction

Studies of the interaction between tides and airglow have focussed almost entirely on nighttime observations. *McDade* [1998] gives a summary of the present understanding of how tidal perturbations in MLT minor constituents can affect nightglow emission rates. In general, these emissions are restricted to a narrow altitude range near the mesopause, and observations only give information about a tidal perturbation as it passes through an emission layer. *Burrage et al.* [1994] showed that variations in the O_2 atmospheric band nightglow at 94 km were consistent with the (1,1) diurnal tide mode. $O(^1S)$ nightglow observations at the equator show variations throughout the night of up to a factor of three at 90km, which have been linked to strong tidal dynamics [*Shepherd et al.*, 1995]. Several modeling studies have concluded that the dominant cause of $O(^1S)$ nightglow variations is advection of atomic oxygen by the diurnal tide in the vertical wind [*Akmaev and Shved*, 1980; *Roble and Shepherd*, 1997; *Ward*, 1998].

In contrast to these narrow nighttime emissions, the atmospheric band $O_2(b^1\Sigma_g \rightarrow X^3\Sigma_g)(0\text{-}0)$ dayglow is at least ten times stronger and extends over a larger altitude range (approx. 50 - 100 km). Daytime emissions are initiated through O_2 photolysis, O_2 resonance scattering, and ozone photolysis [*Wallace and Hunten*, 1968]. The HRDI instrument aboard the Upper Atmosphere Research Satellite (UARS) uses observations of this airglow to measure horizontal wind fields [*Hays et al.*, 1993]. Recently, daytime MLT temperatures and atmospheric band volume emission rates (VERs) have been added to the available HRDI dataset, using an inversion technique discussed by *Ortland et al.* [1998]. This paper will present HRDI VER observations, focusing on daytime variability at the equator, and show how this variability can be successfully modeled using accepted photochemistry and a tidally perturbed reference atmosphere.

Paper number 1999GL900253.
0094-8276/99/1999GL900253$05.00

HRDI Observations

The 57 degree orbit inclination of UARS allows HRDI to observe latitudes to $\pm$ 72 degrees. On any day of observations, HRDI will make up to 15 measurements at a fixed latitude, equally spaced in longitude, all at nearly the same local time. These can be averaged to obtain a zonal mean. Observations precess in local time 20 minutes per day, and an average over a month will cover almost all daylight local times. Figure 1 shows observed monthly average VERs at the equator for March and June 1993. These maps are typical of equinox and solstice observations. For much of the MLT the emission rate exceeds $6\text{x}10^4$ photons cm^{-3} sec^{-1}. June emission rates are symmetric about noon, which is as expected from an emission that mainly originates through absorption of solar radiation. Maximum emission is seen at noon local time, at an altitude of 95 km, when O_2 photolysis rates are at a maximum. In March the pattern of emission is no longer symmetric, with afternoon emission rates exceeding the noon time value. The height of peak emission descends from 92.5 km at noon to 87.5 km at 18 hrs. local time.

Figure 2a shows the latitude structure of the emission at an altitude of 87.5 km for March/April 1993. Variations of almost a factor of 2 are observed, and are symmetric about the equator and anti-symmetric about 2 p.m. local time. Mid-latitude emissions appear to peak earlier in the day, and minimize when the equatorial emission is greatest. Figure 2a is consistent with a diurnal cycle, if viewed in conjunction with the O_2 atmospheric band nightglow brightness map reported by *Burrage et al.* [1994]. Equatorial nightglow emissions maximize shortly after sunset and minimize near sunrise. In addition, the amplitude of the daytime changes is observed to be largest at equinox, when the amplitude

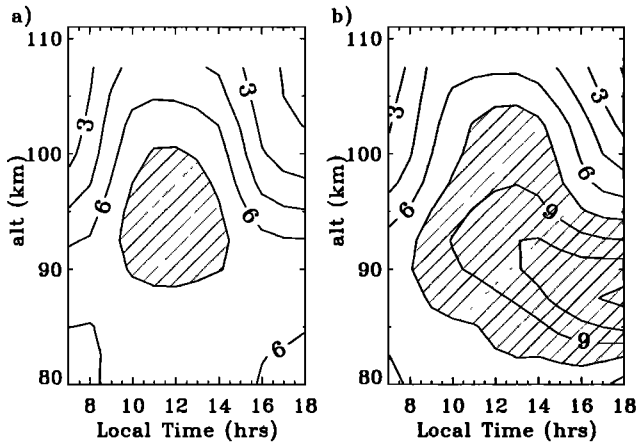

Figure 1. HRDI observed monthly average O_2 atmospheric band volume emission rates (VER) at the equator for a) June and b) March 1993. Contour intervals are every $1.5\text{x}10^4$ photons cm^{-3} s^{-1}. Shaded regions have emission rates in excess of $7.5\text{x}10^4$.

of the diurnal tide is at a maximum. Analysis of data at the same altitude for June/July 1993 shows little variability, with equatorial emissions constant to within 15%.

Model Simulations

A simulated atmospheric band volume emission rate (η) is calculated as the sum of three production terms for $O_2(b^1\Sigma_g)$ [*Bucholtz et al.*, 1986]:

$$\eta = F_c Q \left(g[O_2] + \phi k_1 [O(^1D)][O_2] + P_{Barth} \right). \quad (1)$$

F_c is the Franck-Condon factor for the (0–0) transition, and Q is the proportion of excited O_2 that actually emit a photon, instead of being quenched. The first term on the right of (1) is production via resonance scattering, where g is the radiation absorption rate for the $X^3\Sigma_g \rightarrow b^1\Sigma_g$ transition [*Bucholtz et al.*, 1986; *Mlynczak*, 1993]. The second production term is collisional excitation with $O(^1D)$, where k_1 is the quenching rate of $O(^1D)$ by O_2, and ϕ is the efficiency for production of $O_2(b^1\Sigma_g)$. Reaction rates are taken from *DeMoore et al.* [1997]. The concentration of $O(^1D)$ depends on the photolysis rates of ozone and molecular oxygen:

$$[O(^1D)] = \frac{J_3[O_3] + J_2[O_2]}{k_0[N_2] + k_1[O_2] + A_{1D}}. \quad (2)$$

k_0 is the quenching rate of $O(^1D)$ by N_2, J_3 is the Hartley photolysis rate of ozone, and J_2 is the molecular oxygen photolysis rate in the Schumann-Runge Continuum ($\lambda \leq$ 176 nm). Ultraviolet spectra used to calculate photolysis rates are taken from Solar Ultraviolet Spectral Irradiance Monitor [*Brueckner et al.*, 1993], also on board UARS.

The last production term in (1) is the result of a two-step Barth-type process:

$$\begin{aligned} O + O + M &\rightarrow O_2^* + M \\ O_2^* + O_2 &\rightarrow O_2(b^1\Sigma_g) + O_2 \end{aligned} \quad (3)$$

This term is calculated using the formulation of *McDade et al.* [1986]. During the daytime the maximum contribution from this mechanism occurs near 90 km where it is approximately 10 %, while at 105 km and 80 km the contribution is less than 1 percent. At night the Barth-type mechanism is the only one to operate. The MSISE-90 climatology [*Hedin*, 1991] is used for concentrations of N_2, O_2, $O(^3P)$ and for temperature. Ozone concentrations are calculated using MSIS $O(^3P)$ and assuming ozone is in photochemical equilibrium [*Allen et al.*, 1984].

Simulated VERS are presented for two cases. Firstly, an MSIS atmosphere for June 1993 is used without diurnal tide perturbations. Figure 3a shows a slice through modeled emission rates at the equator. Modeled emission rates are symmetric about noon local time, and are comparable with the June HRDI observations (this is as expected since at solstice diurnal tide amplitudes are low). Modeled emissions peak at a lower altitude than is observed, which may be a result of inaccuracies in reaction rates or modeled constituent densities. For the second case, prior to calculation of daytime VERs, an MSIS atmosphere for March 1993 is perturbed with diurnal tides in temperature, density and vertical wind. Using the method described in the study of nightglow variations by *Yudin et al.* [1998] tidal oscillations in the long-lived species $O(^3P)$ and O_2 are calculated using a linearized continuity equation. The same perturbed atmosphere used in that study is used here to simulate the effect of a diurnal tide on the dayglow. The amplitude and phase of tidal perturbations are obtained from the TMTM after the model is tuned to diurnal meridional wind amplitudes observed by HRDI and the Wind Imaging Interferometer (WINDII) during March 1993 [*Yudin et al.*, 1997, 1998]. Figure 3b shows calculated VERs at the equator, which show the same feature seen in HRDI observations made in March 1993. A descending layer is seen in modeled emission in the afternoon, such that the 87.5 km emission rate at 17 hrs. is 37 % larger than the noon time value. A third run using an unperturbed March 1993 atmosphere does not show the observed afternoon enhancement, and has the same pattern of emission as the June simulations.

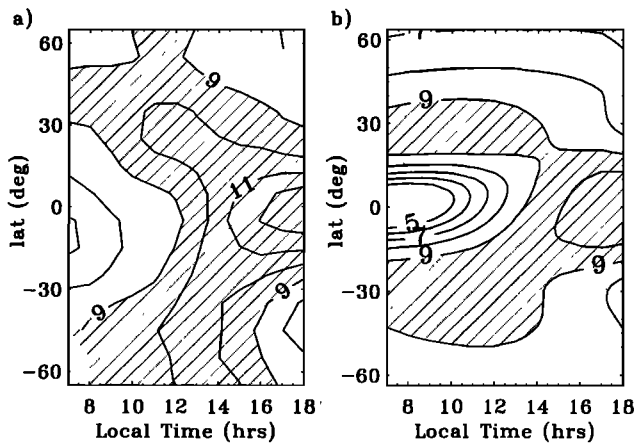

Figure 2. VERs at 87.5 km a) observed mean March/April 1993. Contour intervals are every 10^4 photons cm^{-3} s^{-1}. Shaded regions have emission rates in excess of $9\text{x}10^4$ photons cm^{-3} s–1. b) Modeled VERs calculated using model atmosphere perturbed with estimated diurnal tides for March 1993.

Perturbations due to the vertical wind have, by far, the greatest effect on simulated daytime emission (a model run with vertical wind perturbations turned off actually showed a decrease in afternoon emissions at the equator). This was also shown to be true for simulated $O(^1S)$ and O_2 atmospheric band nightglows [*Yudin et al.*, 1998]. The TMTM calculated vertical wind used in the second case is shown in Figure 4, where it can be seen that around 90 km the tide peaks in the downward direction in the afternoon. A slice of modeled emission rates at 87.5 km is shown in Figure 2b. The latitude structure of changes in emission has the same phase and amplitude as the observations and mirrors the structure of the (1,1) diurnal tide mode. Perturbations in density have a relatively small effect on emission rates. Increases in production of $O_2(b^1\Sigma_g)$ resulting from an increase in O_2 are offset by the simultaneous increase in quenching by N_2. For example, at 86 km a 20 % variation in O_2 would lead to less a 5 % change in VER. The simulation of tidal signatures in the dayglow based on parameters derived from HRDI daytime winds can be considered an important step in confirming the consistency in the daytime HRDI wind and dayglow observations.

Analysis and Conclusion

It is evident from March observations that the asymmetry in emissions cannot be the result of changes in solar radiation (which are symmetric about noon). The latitude structure of the atmospheric band emission near 90 km during equinox is consistent with the diurnal tide structure. The observed afternoon local time enhancement of equatorial emission rate is coincident with the maximum in the downward component of the diurnal tide. Since atomic oxygen concentrations are rapidly increasing with altitude in this region of the atmosphere, a downward wind will advect air richer in atomic oxygen. An enhancement in the atomic oxygen will lead to enhanced emission not only through (3), but also through increased ozone concentrations (2), since increases in atomic oxygen will lead to increased production of ozone through 3-body recombination with molecular oxygen. In fact, 85% of the increase in modeled emission at 87.5 km is a result of increased ozone, and hence photolytic production of $O(^1D)$.

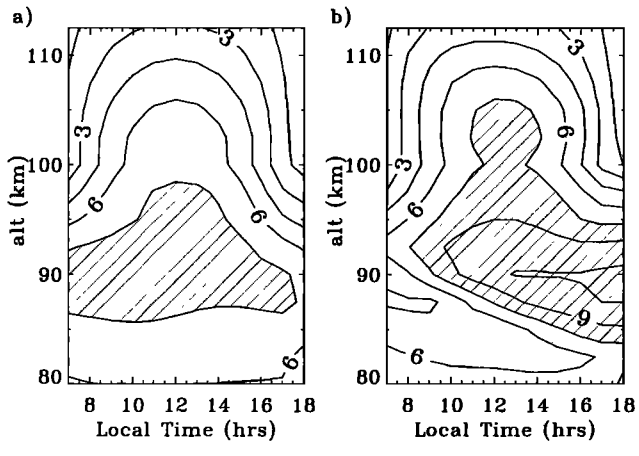

Figure 3. Modeled VERs (cm^{-3} s^{-1}) at the equator for a) June, and b) March, 1993. Same contour intervals as Figure 1.

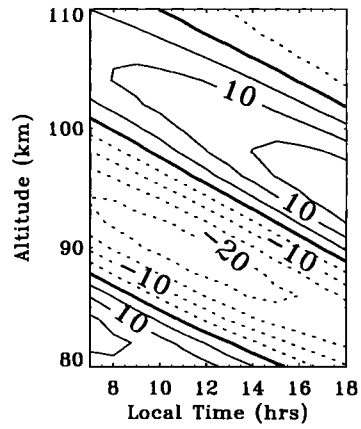

Figure 4. TMTM diurnal tide component of the vertical wind (cm s^{-1}) for model tuned to March 1993 observations. Negative values denote downward direction.

The tidally driven afternoon enhancement in ozone prompts a new interpretation of the Solar Mesosphere Explorer (SME) ozone measurements. SME observed a semiannual cycle in 0.006 mbar ozone at the equator, with peaks at equinox [*Thomas*, 1990]. *Garcia and Solomon* [1985] argued that the seasonal variability in ozone is a result of seasonal changes in turbulent mixing due to gravity wave breaking. However, since SME observations were always at approximately 16 hrs. local time, these measurements were made during the time of maximum downward advection of air rich in atomic oxygen. Therefore, the observed seasonal variation could instead be a result of seasonal variation in the amplitude of the tide. Further study is needed to resolve whether ozone variability at the equator is a tidal phenomenon.

In conclusion, HRDI observations of the O_2 atmospheric band dayglow provide a means to extend analysis of tidal influences on MLT composition into the daytime. Tidal signatures in daytime emission rates are consistent with nighttime observations, and the observed afternoon enhancement at equinox has been successfully modeled as the result of increased ozone concentrations due to tidal vertical advection of atomic oxygen from the Lower Thermosphere. Since the amplitude and phase of the modeled diurnal tide vertical wind were derived from independent HRDI measured zonal winds, HRDI observations are shown to be self-consistent.

Acknowledgment. This work is sponsored by NASA through contract NAG 5-6709.

References

Akmaev, R.A., and G.M. Shved, Modelling of the composition of the lower thermosphere taking account of the dynamics with application to tidal variations of the [OI] 5577Å airglow, *J. Atmos. Terr. Phys.*, 42, 705-716, 1980.

Allen, M., Lunine, J.I., Y.L.Yung, The vertical distribution of ozone in the mesosphere and lower thermosphere, *J. Geophys. Res.*, 89, 4,841-4,872, 1984.

Brueckner, G.E., K. Edlow, L. Floyd, J. Lean, and M. VanHoosier, The Solar Ultraviolet Spectral Irradiance Monitor (SUSIM) experiment on board the Upper Atmosphere Research Satellite (UARS), *J. Geophys. Res.*, 98, 10,695-10,711, 1993.

Bucholtz, A., W.R. Skinner, V.J. Abreu, and P.B. Hays, The dayglow of the O_2 atmospheric band system, *Planet. Space. Sci.*, 34, 1031-1035, 1986.

Burrage, M.D., N. Arvin, W.R. Skinner, and P.B. Hays, Observations of the O_2 atmospheric band nightglow by the High Resolution Doppler Imager, *J. Geophys. Res.*, 99, 15,017-15,023, 1994.

DeMore, W.B., S.P.Sander, C.J. Howard, A.R. Ravishankara, D.M. Golden, C.E. Kolb, R.F. Hampson, M.J. Kurylo, M.J. Molina, Chemical kinetics and photochemical data for use in stratospheric modeling, evaluation number 12, JPL Publication 97-4, 1997.

Garcia, R.R., and S. Solomon, The effect of breaking gravity waves on the dynamics and chemical composition of the mesosphere and Lower thermosphere, *J. Geophys. Res.*, 90, 3850-3868, 1985.

Hays, P.B., V.J. Abreu, M.E. Dobbs, D.A. Gell, H.J. Grassl, and W.R. Skinner, The High Resolution Doppler Imager on the Upper Atmosphere Research Satellite, *J. Geophys. Res.*, 98, 10,713-10,723, 1993.

Hedin, A.E., Extension of the MSIS thermosphere model into the middle and lower atmosphere, *J. Geophys. Res.*, 96, 1159-1172, 1991.

McDade, I.C., D.P. Murtagh, R.G.H. Greer, P.H.G. Dickinson, G. Witt, J. Stegman, E.J. Llewellyn, I. Thomas, and D.B. Jenkins, ETON 2: Quenching parameters for the proposed precursors of $O_2(b^1\Sigma_g^+)$ and $O(^1S)$ in the terrestrial nightglow, *Planet. Space. Sci.*, 34, 789-800, 1986.

McDade, I.C., The photochemistry of the MLT oxygen airglow emissions and the expected influences of tidal perturbations, *Adv. Space. Res.*, 21, 787-794, 1998.

Mlynczak, M.G., An evaluation of the rate of absorption of solar radiation in the $O_2(X^3\Sigma_g \rightarrow b^1\Sigma_g)$ transition, *Geophys. Res. Lett.*, 20, 1439-1442, 1993.

Ortland, D.A., P.B. Hays, W.R. Skinner, and J.-H. Yee, Remote sensing of mesospheric temperatures and $O_2(^1\Sigma)$ band volume emission rates with the high resolution doppler imager, *J. Geophys. Res.*, 103, 1821-1835, 1998.

Roble, R.G. and G.G. Shepherd, An analysis of wind imaging interferometer observations of $O(^1S$ equatorial emission rates using the thermosphere-ionosphere-mesosphere-electrodynamics general circulation model, *J. Geophys. Res.*, 102, 2467-2474, 1997.

Shepherd, G.G., C. McLandress, and B.H. Solheim, Tidal influence on $O(^1S)$ airglow emission rate distributions at the geographic equator as observed by WINDII, *Geophys. Res. Lett.*, 22, 275-278, 1995.

Thomas, R.J., Seasonal ozone variations in the upper atmosphere, *J. Geophys. Res.*, 95, 7395-7401, 1990.

Wallace, L., and D.M. Hunten, Dayglow of the Oxygen A Band, *J. Geophys. Res.*, 73, 4813-4834, 1968.

Ward, W., Tidal mechanisms of dynamical influence on oxygen recombination airglow in the mesosphere and lower thermosphere, *Adv.Space.Res.*, 21, 795-805, 1998.

Yudin, V.A., B.V. Khattatov, M.A. Geller, D.A. Ortland, C. McLandress, G.G. Shepherd, Thermal tides and studies to tune the mechanistic tidal model using UARS observations, *Ann.Geophys.*, 15, 1205-1220, 1997.

Yudin V.A., M.A. Geller, B.V. Khattatov, D.A. Ortland, M.D. Burrage, C. McLandress, G.G. Shepherd, TMTM simulations of tides: comparison with UARS observations, *Geophys. Res. Lett.*, 25, 221-224, 1998.

Daniel Marsh, Department of Atmospheric, Oceanic, and Space Science, University of Michigan, Ann Arbor, MI 48109. (e-mail: danielm@umich.edu)

(Received December 2, 1998; revised February 26, 1999; accepted March 24, 1999.)